& Hirs, C. (1968) *J. Biol. Chem. 243*, 6482–6494.
Saxholm, H. J. K., & Pitot, H. C. (1974) *Biochim. Biophys. Acta 562*, 386–397.
Sober, H. A., Ed. (1970) *Handbook of Biochemistry, Selected Data for Molecular Biology*, p C47, CRC Press, Cleveland, OH.
Varma, R., Varma, R. S., & Wardi, A. H. (1973) *J. Chromatogr. 77*, 222–227.
Vennegoor, C. J., & Bloemendal, H. (1972) *Eur. J. Biochem. 26*, 462–473.

Crystal Structure Determinations of Coenzyme Analogue and Substrate Complexes of Liver Alcohol Dehydrogenase: Binding of 1,4,5,6-Tetrahydronicotinamide Adenine Dinucleotide and *trans*-4-(*N*,*N*-Dimethylamino)cinnamaldehyde to the Enzyme†

Eila Cedergren-Zeppezauer,* Jean-Pierre Samama,‡ and Hans Eklund

ABSTRACT: 1,4,5,6-Tetrahydronicotinamide adenine dinucleotide (H_2NADH) has been used as a reduced coenzyme analogue to study a simulated transient intermediate of liver alcohol dehydrogenase (LADH) with *trans*-4-(*N*,*N*-dimethylamino)cinnamaldehyde (DACA) as a substrate. X-ray diffraction data of two crystal modifications have been analyzed to 2.9-Å resolution: an orthorhombic complex where the coenzyme analogue binds to the apoenzyme conformation [Eklund, H., Nordström, B., Zeppezauer, E., Söderlund, G., Ohlsson, I., Boiwe, T., Söderberg, B.-O., Tapia, O., Bränden, C.-I., & Åkesson, Å. (1976) *J. Mol. Biol. 102*, 27–57] and a triclinic complex with coenzyme and substrate bound to the holoenzyme conformation [Eklund, H., Samama, J.-P., Wallén, L., Brändén, C.-I., Åkesson, Å., & Jones, T. A. (1981) *J. Mol. Biol. 146*, 561–587]. The interpretation of difference electron density maps for both crystal modifications is based on calculations where the phase angles have been derived from refined enzyme models. H_2NADH binds to the coenzyme binding domain in an extended conformation. The tetrahydronicotinamide ring is situated within the active site region in both enzyme conformations, but the orientation of the ring plane in relation to the active site zinc atom is very different. In the triclinic LADH–H_2NADH–aldehyde complex the coenzyme analogue binds in a similar way as NADH to a ternary inhibited complex. The combined effect of the presence of H_2NADH and the large DACA substrate triggers the gross conformational change of the protein, which involves the movement of the catalytic domains in the dimeric molecule. In contrast, only local structural changes in the orthorhombic LADH–H_2NADH complex are observed upon coenzyme analogue binding. A network of hydrogen bonds between water molecules, the coenzyme, and side chains from the catalytic domain bridges the cleft between the domains in the orthorhombic complex. Since the conformational change narrows the cleft, no such water arrangement is found in the triclinic substrate complex. In the orthorhombic complex the substrate binding pocket is occupied by a methylpentanediol (MPD) molecule used as the precipitating agent during crystallization. MPD binds within hydrogen-bonding distance to zinc-bound water. The X-ray analysis shows that the aldehyde molecule is directly liganded to the metal atom in the triclinic LADH–H_2NADH–DACA complex. The binding of the chromophoric aldehyde substrate within the single crystals used for diffraction experiments was monitored by microspectrophotometric measurements.

Alcohol dehydrogenase from horse liver (LADH)[1] is known to undergo conformational changes upon coenzyme and substrate binding. These changes result in a rotation of the catalytic domains with respect to a central core, the coenzyme binding domains in the dimeric molecule (Eklund et al., 1981). This core structure, however, is virtually identical with that of the unliganded enzyme structure. One functionally important role of the conformational difference is that the coenzyme and substrate clefts become narrower and less accessible to solvent. Our interest has been to investigate the factors that influence this conformational transition. The importance of the proper positioning of the nicotinamide ring has been demonstrated in earlier investigations. Thus the protein remains in the apoenzyme conformation in the complex with pyridine adenine dinucleotide, where the carboxamide group is absent (Samama et al., 1977). There is a similar conformation in the complex with the inactive analogue 5-methylpyridine adenine dinucleotide, where steric repulsion between the methyl group and the protein prevents proper positioning of the nicotinamide ring (Samama et al., 1981). In both these complexes the bound coenzyme analogues are folded in a nonproductive binding manner such that the pyridinium ring is located 20 Å from the catalytic zinc atom; this is called the "surface fold".

Other studies have shown the importance of the environment of the catalytic zinc atom. Thus the active coenzyme analogue 3-iodopyridine adenine dinucleotide binds with the surface fold when the aldehyde competitive inhibitor imidazole is bound to the catalytic zinc atom. The corresponding complex with the inhibitor dimethyl sulfoxide (Me_2SO) bound to zinc gives

† From the Swedish University of Agricultural Sciences, 750 07 Uppsala 7, Sweden. *Received February 24, 1982.* This work was supported by Grant 2767 from the Swedish Natural Science Research Council and by funds from the Centre National de la Recherche Scientifique.

‡ Present address: Institut de Chimie, Université Louis Pasteur de Strasbourg, Strasbourg, France.

[1] Abbreviations: Tris, tris(hydroxymethyl)aminomethane; MPD, 2-methyl-2,4-pentanediol; DACA, *trans*-4-(*N*,*N*-dimethylamino)cinnamaldehyde; H_2NADH, 1,4,5,6-tetrahydronicotinamide adenine dinucleotide; Me_2SO, dimethyl sulfoxide; enzyme, horse liver alcohol dehydrogenase (LADH; EC 1.1.1.1).

0006-2960/82/0421-4895$01.25/0

triclinic crystals (Samama, 1979) with the protein in the holoenzyme conformation. In order to explore the role substrates play in the LADH conformational change, we have studied the ternary complex involving enzyme and 1,4,5,6-tetrahydronicotinamide adenine dinucleotide (H_2NADH) with the chromophoric substrate *trans*-4-(*N*,*N*-dimethylamino)-cinnamaldehyde (DACA) (Dunn & Hutchison, 1973; Dunn et al., 1975). The inactive coenzyme analogue, H_2NADH, and the real substrate, DACA, form a simulated transient complex that provides a suitable model for studying substrate binding to LADH. This complex has the same absorption characteristics as the transient intermediate formed with NADH. Since the H_2NADH complexes are very stable we have utilized this property to perform a crystallographic investigation of the orthorhombic complex LADH–H_2NADH and the triclinic complex LADH–H_2NADH–DACA to 2.9-Å resolution. The spectrum of the transient complex with λ_{max} = 468 nm was measured to unambiguously identify the chemical species present in the crystals used in the crystallographic experiments (Bignetti et al., 1979).

Materials and Methods

The coenzyme analogue 1,4,5,6-tetrahydronicotinamide adenine dinucleotide, H_2NADH, was prepared by a modification of the method of Biellmann & Jung (1971) and kindly supplied to us by Dr. Guy Branlant, Institut de Chimie, Strasbourg, France, at an early stage in this work and later by Leif Wallén, Department of Chemistry and Molecular Biology, Swedish University of Agricultural Science. The product was analyzed by UV, proton NMR, and ^{13}C NMR spectroscopy (G. Branlant, B. Eiler, L. Wallén, and J.-F. Biellmann, unpublished experiments) and was stable at pH 9 according to the UV spectral criteria. *trans*-4-(*N*,*N*-Dimethylamino)cinnamaldehyde, DACA, was purchased from Aldrich, sublimated, and used immediately. Tris salt (from Serva, Heidelberg, Federal Republic of Germany) and HCl (suprapure from Merck) were used without further purification. 2-Methyl-2,4-pentanediol, MPD (lot B6B, Eastman Kodak Co.), was doubly distilled under purified nitrogen and stored in the dark at 4 °C. Buffers were prepared by using twice-distilled water.

Crystallization of Enzyme Complexes. (*a*) *Crystals Obtained in the Presence of Low Substrate Concentration.* Purified horse liver alcohol dehydrogenase (EE isozyme) was kindly provided by Dr. Å. Åkesson, Karolinska Institutet, Stockholm, Sweden. One-milliliter enzyme samples placed in washed dialysis bags were dialyzed against Tris-HCl (0.05 M, pH 9.5) with several replacements of fresh buffer. During the last step of the dialysis a single enzyme sample with 10 mg (0.125 mM) of enzyme was placed in 5 mL of buffer containing 6 mg (1.7 mM) of H_2NADH and 25 μg of (0.020 mM) DACA substrate. The free substrate in solution has an absorption maximum at 398 nm. Bound to alcohol dehydrogenase in the presence of NADH or H_2NADH, a new chromophore is formed with λ_{max} at 464 and 468 nm, respectively (Dunn & Hutchison, 1973; Dunn et al., 1975). After substrate addition, a strong orange color developed inside the dialysis bag and the outer solution became decolorized. Aliquots were withdrawn from the enzyme complex solution before adding precipitant to examine the spectral properties of the complex. Small additions of methylpentanediol, MPD, over a 3-week period gave pale yellow, orthorhombic crystals that began to grow at 12% (v/v) MPD. The strong chromophore at 468 nm initially formed, and the subsequent bleaching was easily observed by eye. Crystals were harvested at a final concentration of 20–30% (v/v) precipitant. No microspectrophotometric measurements were made on single crystals from these crystallization experiments before the X-ray analysis. Throughout this work, all steps in the preparation of crystals, including X-ray data collection, were performed at 4 °C.

(*b*) *Crystals Obtained in the Presence of High Substrate Concentration.* The treatment of the enzyme solutions was the same as in case a. The complex was formed by placing a dialysis bag containing 10 mg (0.125 mM) of enzyme into 6 mL of outer dialysate containing 3.6 mg (0.85 mM) of H_2NADH and 500 μg of (0.46 mM) DACA. Within 1 h a color change was observed inside the dialysis bag, indicating the formation of the chromophore at 468 nm. Precipitation with MPD started after 12-h dialysis, and orange, triclinic crystals began to grow at 17–21% (v/v) MPD. The final concentration of precipitant was 30% (v/v). Absorption spectra were recorded on single crystals isolated from the same batch of crystals used for the X-ray analysis. LADH–NADH crystals were prepared according to procedures described by Bignetti et al. (1979), and they belong to the triclinic space group.

Microspectrophotometric Measurements. Absorption spectra were measured on a Leitz microspectrophotometer at the University of Parma, on triclinic crystals from the same batch as that used for the 4.5-Å data set (Bignetti et al., 1979). During data collection on the high-resolution part of the 2.9-Å data set, absorption spectra were recorded on a Zeiss UMSPI at the Karolinska Institute, Stockholm, Sweden. A crystal suspension was placed on a quartz depression slide, and the quartz cover slip was fastened with wax or glue to avoid evaporation of the mother liquid. The preparation of samples was made in the cold room whereas spectra were recorded at 23 °C. The maximum distance between the quartz plates was 1 mm, and the diameter of the light beam was either 8 or 20 μm. The centering of the crystal on the microscope was accurate to within a few microns. Since unpolarized light was used no quantitative determinations of substrate concentrations were made. Absorption spectra of LADH–NADH crystals into which the substrate had been diffused were compared with crystals of the LADH–H_2NADH–DACA complex crystallized from a solution as described above (case b).

X-ray Analysis. X-ray intensities were collected on a Stoe four-circle diffractometer and corrected for absorption, Lorentz, and polarization effects and time-dependent intensity decreases as described in detail previously (Eklund et al., 1976). Scale factors and minor corrections for anisotropic intensity decreases (Eklund et al., 1981) due to crystal disorder were calculated for each crystal. The orthorhombic LADH–H_2NADH data set was compared with the data for the native enzyme and the triclinic LADH–H_2NADH–DACA data set with the data for the LADH–NADH–Me_2SO complex (Eklund et al., 1981). For each crystal R values were calculated where

$$R = \sum_{hkl} ||F_p| - s|F_{DER}| \exp-(u_1h^2 + u_2k^2 + u_3l^2)| / \sum_{hkl} |F_p|$$

in the orthorhombic case. F_p denotes structure factors for the protein, F_{DER} denotes the structure factors for the complex, and s is the scale factor. The exponential term in the triclinic case is $-(u_1h^2 + u_2k^2 + u_3l^2 + u_4kl + u_5hl + u_6hk)$ where u_1–u_6 are the anisotropic disorder parameters. The variation in R scatters between 8.7 and 12.6% for orthorhombic and triclinic data sets.

(*a*) *Orthorhombic Data Set.* The crystals belong to the space group $C222_1$ with cell dimensions a = 56.0 Å, b = 75.2 Å, and c = 181.7 Å. Nine different crystals of the complex,

crystallized at low substrate concentration, were used to collect the 8570 independent reflections to 2.9-Å resolution. Three types of difference Fourier maps were calculated and interpreted: (1) F_{obsd}(complex) − F_{obsd}(native)α_{calcd}; (2) F_{obsd}(complex) − F_{calcd}(native)α_{calcd}; (3) $2F_{obsd}$(complex) − $F_{calcd}\alpha_{calcd}$. The phase angles were obtained after crystallographic refinement of the native LADH structure. The crystallographic R value of the native model, defined as $\sum||F_{obsd}| - |F_{calcd}||/\sum|F_{obsd}|$, is 20% at this stage (T. A. Jones, unpublished results). The model building and examination of Fourier maps were carried out on a Vector General 3404 interactive graphics display system with the RING and FRODO programs (Jones, 1978, 1982). The type 1 and type 2 difference maps were used to interpret the binding of the H_2NADH molecule from which the model was built. Furthermore, the type 1 map was used to list regions where strong positive and negative peaks indicated that there were differences in details of the protein model. For model building of these differences type 3 maps were used.

The type 2 difference map was used to examine whether electron density appeared at positions in the structure where the native enzyme model was poorly defined. Side chains are ill-defined for a number of surface amino acids, particularly in the vicinity of the large, open coenzyme binding cleft, and thus were not included in the structure factor calculation for the native protein. In the complex structure we found that several of these side chains were oriented in fixed positions and therefore were included. The electron densities for the coenzyme analogue, one precipitant molecule (MPD), and the water molecules in the active site were also interpreted from this map since nothing but the protein model contributed to the phasing. Excellent agreement was obtained between H_2NADH models interpreted from type 1 and type 2 maps. Standard bond distances for the tetrahydronicotinamide ring were used from the work of Hope (1969).

The model building of the differences in the protein structure, induced by the binding of the analogue, was made from type 3 maps. A stepwise procedure was performed. Atomic coordinates for the coenzyme analogue molecule and MPD, rigidly oriented side chains, and shifts in atomic positions for the protein model were introduced in structure factor calculations, whereby the native enzyme phase angles were gradually modified. In cases where the enzyme model did not coincide with the difference electron density it was easy, by means of the model building program FRODO, to break any bonding connections in the model and bring atoms into density. Good stereochemistry was maintained by immediately regularizing the model. Structure factors were calculated by using the PROTEIN program of Steigemann. In the final model of the LADH–H_2NADH–MPD complex 95% of the total number of atoms of the protein (374 amino acids and two Zn atoms) plus the H_2NADH and MPD molecules were included in the calculation. A crystallographic R value of 25% was obtained. No further refinement of the complex was made. A difference electron density map was calculated by using the amplitudes F_{obsd}(LADH–H_2NADH) − F_{obsd}(LADH–ADP-ribose) and calculated phases in order to further verify the position of the tetrahydronicotinamide ring of the analogue interpreted from type 1 and type 2 Fourier maps. The data of B. Nordström (Abdallah et al., 1975) were used and scaled against the observed amplitudes for the LADH–H_2NADH complex.

(*b*) *Triclinic Data Set.* The crystals belong to the space group $P1$ and have cell dimensions a = 52.0 Å, b = 44.5 Å, c = 94.2 Å, α = 104.4°, β = 102.2°, and γ = 70.7°. Fifteen

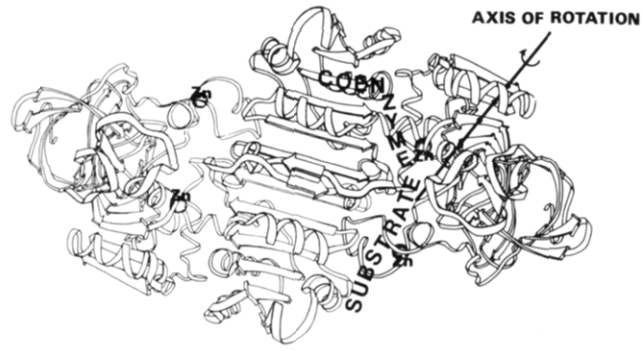

FIGURE 1: Schematic drawing of the LADH dimer, designed by Bo Furugren. The central part of the molecule illustrates the two coenzyme binding domains bound together across a 2-fold axis perpendicular to the plane of the paper. The two catalytic domains are separated from this central part by the coenzyme and substrate binding clefts. The binding sites for the coenzyme and substrate have been indicated for one of the subunits. The metal binding sites are located at the fringes of the catalytic domains. The transition of LADH from the apo to the holo conformation takes place through a domain rotation. The rotation axis is marked, and the arrow specifies the direction of the rotation.

crystals of the complex LADH–H_2NADH–DACA, crystallized at high substrate concentration, were used to collect the 16 416 independent reflections corresponding to 2.9-Å resolution. Intensities were corrected as described above. Difference electron density maps were calculated with the amplitudes $F_{obsd} - F_{calcd}$ by using phase angles derived from the refined triclinic holo structure, LADH–NADH–Me_2SO (Eklund et al., 1981). The crystallographic R value of the holo structure is 25% at this stage of the refinement, and each subunit of the dimeric protein has been refined independently (H. Eklund and T. A. Jones, unpublished results). In the subsequent calculations reported here the subunits were also treated independently. The coenzyme analogue binding was interpreted from a difference Fourier map with the following terms: F_{obsd}(LADH–H_2NADH–DACA) − F_{calcd}(LADH–holoprotein)α_{calcd}. No contribution from bound NADH to the phase angles in the triclinic model was included. Shifts in the protein part of the complex could be deduced from this map. The coordinates for the H_2NADH model were introduced in a structure factor calculation, and a second Fourier map was calculated, F_{obsd}(LADH–H_2NADH–DACA) − F_{obsd}(H_2NADH plus holo-LADH)α_{calcd}, and used for the interpretation of the substrate binding. The same procedures as those described for the orthorhombic complex were employed. Stereo diagrams were plotted on a Hewlett-Packard plotter in conjunction with the VG 3404 graphics system by using computer programs written by Dr. T. A. Jones. Coordinates for the orthorhombic and triclinic complexes are available at the Brookhaven Data Bank.

Results

Description of Ligand Binding to the Apo- and Holoenzyme Conformations of LADH. (*a*) *Binding of H_2NADH and MPD to the Orthorhombic Apoenzyme Conformation.* One coenzyme analogue molecule binds per subunit. The subunit consists of two domains separated by a wide cleft that forms the ligand binding site. A schematic representation of the LADH dimer is shown in Figure 1, where the coenzyme and substrate binding sites are indicated for one subunit. The ADP-ribose portion of the H_2NADH molecule coincides with the ADP-ribose density presented in earlier work (Nordström & Brändén, 1975; Abdallah et al., 1975). The difference density is continuous from the adenine pocket to the vicinity of the active site zinc region, and it is possible to fit a model

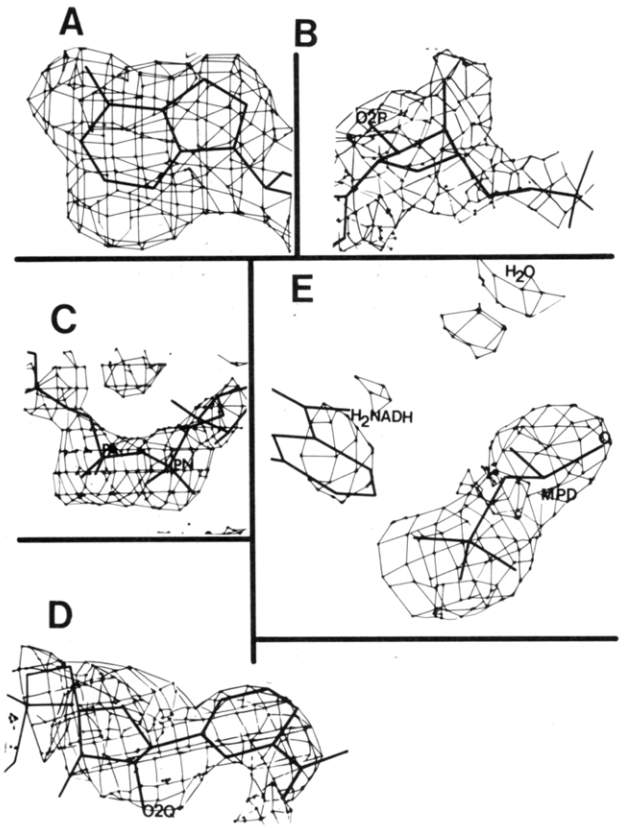

FIGURE 2: Parts of the difference electron density map F_{obsd}-(LADH–H_2NADH–MPD) – F_{calcd}(LADH–native protein) of the 2.9-Å resolution orthorhombic complex. The phase angles are derived from the refined native enzyme model determined to 2.4-Å resolution. (A) Adenine ring; (B) adenosineribose with the connecting density to the pyrophosphate bridge; (C) the pyrophosphate bridge; (D) the tetrahydronicotinamide moiety; (E) the precipitant alcohol, MPD, and part of the density for zinc-bound water. The contoured map with the superimposed model is photographed directly from the display screen and presented in segments due to space limitations in the picture system.

of the whole H_2NADH molecule within this density (Figure 2). Differentiated features in the density are observed, the clearest example being O3′ of the adenosine ribose, the density of which protrudes out of an otherwise flattened feature (Figure 2B). For the O3′ of the second ribose and one atom in the carboxamide group no density is visible at the contour level choosen in Figure 2D.

The environment of the adenine ring of H_2NADH is illustrated in Figure 3A. The side chains of Val-222, Ile-224, Val-268, Ile-269, Phe-198, and Pro-243 line the cavity and Arg-271 approaches N10 of the adenine ring. Ile-224, Asn-225, and Arg-271 could be identified in well-defined density in the enzyme analogue complex, whereas they are poorly defined in the unliganded native structure.

In our model the adenosine ribose is puckered C2′ endo in an "anti" conformation about the glycosidic bond. The puckering was determined by the fit of the model to the difference density and by the interaction with Asp-223. O2′ is within hydrogen-bonding distance to the aspartate and O3′ to NE of Lys-228. So far the interactions between coenzyme and protein are virtually the same for the orthorhombic and triclinic complexes (Eklund et al., 1981). Although a large conformational change in the protein distinguishes these two enzyme forms, those residues that are responsible for the interactions with the adenosine part of the coenzyme are not affected to any appreciable extent by this conformational change.

Table I: Conformation of 1,4,5,6-Tetrahydronicotinamide Adenine Dinucleotide (H_2NADH) and ADP-ribose[a] Bound to Liver Alcohol Dehydrogenase

	orthorhombic complexes		triclinic complex[b]
	ADP-ribose	H_2NADH	H_2NADH
χ_A = C4A–N9A–C1R–C2R	143	148	134
ψ_A = C3R–C4R–C5R–O6R	−108	−109	−104
Φ_A = C4R–C5R–O6R–PA	98	97	129
ω_A = C5R–O6R–PA–OP3	161	148	113
θ_A = O6R–PA–OP3–PN	50	79	95
θ_N = O6Q–PN–OP3–PA	−115	−61	−162
ω_N = C5Q–O6Q–PN–OP3	−37	−122	62
Φ_N = C4Q–C5Q–O6Q–PN	172	99	−159
ψ_N = C3Q–C4Q–C5Q–O6Q	40	−39	48
χ_N = C2N–N1N–C1Q–C2Q		46	137
adenosine ribose puckering	C2′ endo	C2′ endo	C2′ endo
tetrahydronicotinamide ribose puckering		C2′ endo	C2′ endo

[a] The symbol convention is taken from Sundaralingam (1975). The data for the ADP-ribose conformation are based on an interpretation of a recalculated difference electron density map to 2.9-Å resolution using the observed amplitudes measured by Nordström (Abdallah et al., 1975) and calculated phase angles from the refined native enzyme structure to 2.4-Å resolution. [b] The averaged value for the two subunits.

The phosphate positions of H_2NADH correspond to the highest difference peaks in the Fourier maps. This is important because the well-defined positions of the phosphates aid in restricting the possibilities for building the H_2NMN part of the model. The AMP phosphate forms a salt bridge with Arg-47 and appears in high electron density in the complex. The corresponding density is absent in the unliganded LADH. The second phosphate makes contacts with main chain nitrogen atoms (residues 202 and 203) and two water molecules. The width of the cleft between the catalytic and the coenzyme binding domains is approximately 10–12 Å in this region. Water molecules fill up the region between the pyrophosphate group and the catalytic domain. Arg-369 and the internal Glu-68 form a salt bridge within the catalytic domain similar to the unliganded enzyme; Arg-369 does not participate directly in coenzyme analogue binding. Figure 3B shows the environment around the pyrophosphate bridge. The site is hydrophilic and has a nitrogen-rich region, with main chain nitrogen atoms from a helix turn with the sequence GLGGVG, and an oxygen-rich region, consisting of water and carbonyl oxygens. An overall view of the relationship between the H_2NADH position, residues of the catalytic domain, the active site zinc atom, and the water structure is shown in Figure 3C.

From the difference electron density alone it is not possible to unambiguously assign the puckering of the tetrahydronicotinamide ribose. We have built our model C2′ endo, which corresponds to the best fit and avoids too close contacts to protein atoms. O3′ is within hydrogen-bonding distance to the carbonyl oxygen of residue 269, and the ribose ring makes contacts with main chain atoms of residues 269 and 293 (see Figure 4).

The tetrahydronicotinamide ring was fitted to the remainder of the continuous density with the result that the ring is not situated at the immediate neighborhood of the active site zinc center but points toward the domain–domain interaction area comprising residues 51–56—from the catalytic domain—and residues 293–297—from the coenzyme binding domain. The torsion angle χ_N (Table I) is small and very different from the torsion angle observed in coenzyme bound to triclinic LADH. A similar value has recently been observed for NADPH in the glutathione reductase complex with flavin

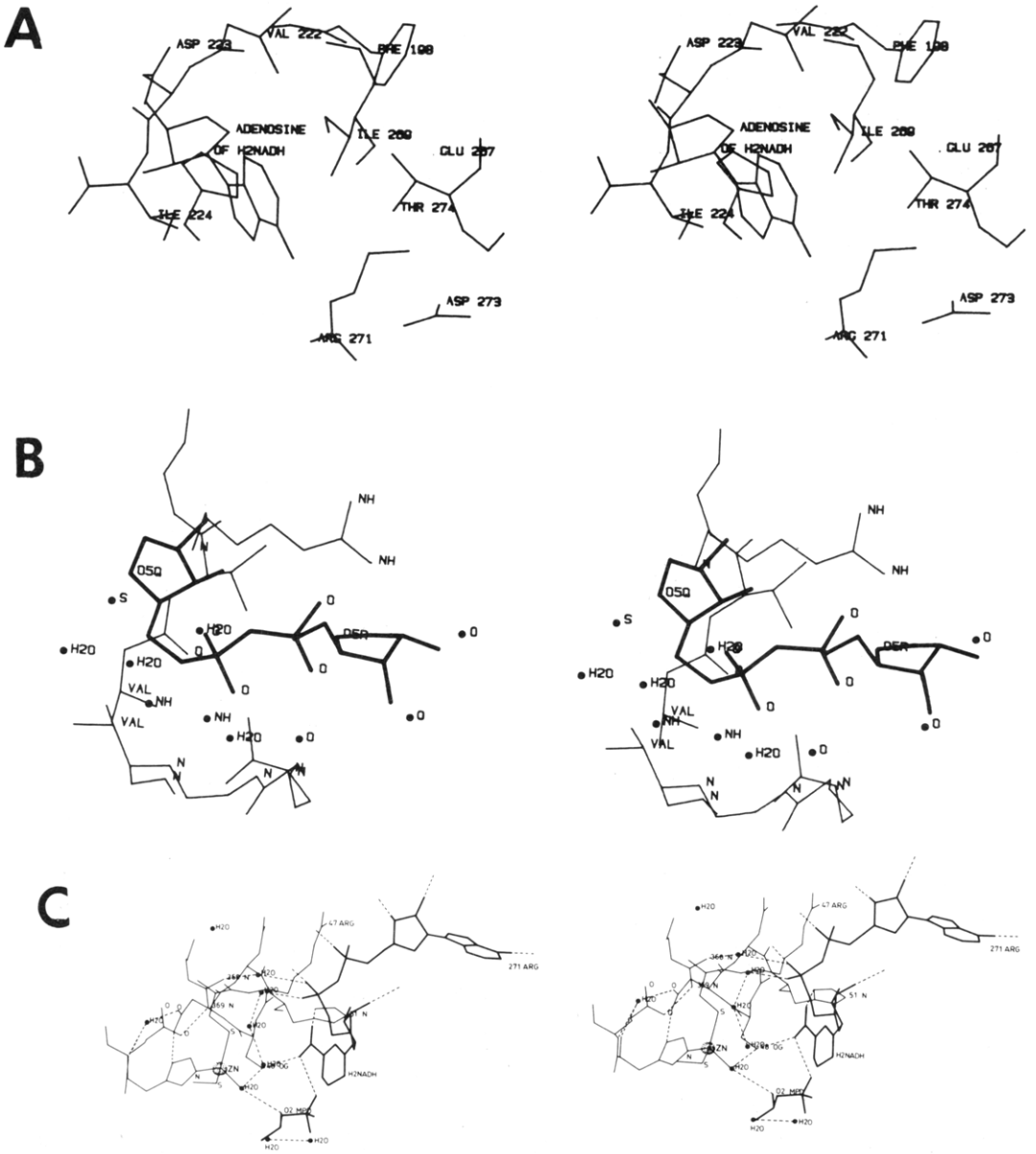

FIGURE 3: Stereo diagram showing the binding of H_2NADH and MPD to orthorhombic LADH. (A) The adenine pocket; (B) the environment within a 6.5-Å radius around OP3 of the pyrophosphate bridge; (C) the whole coenzyme analogue molecule, the active site, and the groups in the catalytic domain that interact directly or indirectly with the ligands. Dashed lines indicate possible hydrogen bonds or salt bridges. Water positions shown in these pictures are listed in Table III.

mononucleotide and NADPH (G. Schulz, personal communication). To further verify that the position of the ring was correct, we calculated a difference map between the LADH–H_2NADH and the LADH–ADP-ribose complexes (data not shown). A strong positive peak of this map clearly superimposes onto the tetrahydronicotinamide ring in our H_2NADH model. The ring is in van der Waals contact with main chain atoms of the peptide segment 293–295 (Figure 4). The position of the ring is of particular interest since the carboxamide group interacts with His-51 and Ser-48. Coordinates for H_2NADH are listed in Table II.

The introduction in structure factor calculations of coordinates for the coenzyme analogue model and the new positions for protein residues in the complex structure gradually modified the phases to become enzyme–complex phase angles. As a last step in the examination of Fourier maps the active site region and the remaining space between domains were inspected since electron density was observed, which could be assigned to neither protein nor H_2NADH. The orthorhombic crystals were grown from an orange solution that initially contained the simulated transient complex. The crystals used for X-ray analysis were pale yellow and the crystallization solution was bleached upon addition of the precipitant alcohol, MPD. (The possible reason for this is discussed later.) In the electron density maps (type 2 and type 3), strong density is found in the substrate cleft at a distance 5 Å away from the catalytic zinc center. This density, which is also present in the native enzyme, extends into the substrate channel composed of leucines and isoleucines. We have interpreted this as an MPD molecule. The fit of a model is shown in Figure 2E. Zinc-bound water makes contact with one of the OH groups of the diol, and the second OH can be oriented toward the carboxamide group of H_2NADH (Figure 3C). Coordinates for the MPD model are found in Table II.

(*b*) *Catalytic Zinc Sphere and Assignment of Bound Water to the Orthorhombic LADH–H_2NADH–MPD Complex.* In the refined native enzyme structure, water positions have been located (T. A. Jones, unpublished data) at interior positions of the protein, at cleft regions between domains, and on the surface of the molecule. The same was done for the LADH–

Table II: Coordinate List in Angstrom Units of 1,4,5,6-Tetrahydronicotinamide Adenine Dinucleotide (H_2NADH), 2-Methyl-2,4-pentanediol (MPD), and *trans*-4-(*N*,*N*-Dimethylamino)cinnamaldehyde (DACA)[a]

orthorhombic LADH-H_2NADH-MPD complex				triclinic LADH-H_2NADH-DACA complex		
H_2NADH			atom	H_2NADH		
X	*Y*	*Z*	name	*X*	*Y*	*Z*
16.3	3.8	36.6	N1A	16.4	3.9	35.8
16.7	4.9	36.0	C2A	17.1	5.0	35.3
16.8	5.2	34.7	N3A	17.0	5.6	34.2
16.2	4.2	34.0	C4A	16.2	4.9	33.3
15.7	3.0	34.4	C5A	15.5	3.7	33.6
15.8	2.8	35.8	C6A	15.6	3.2	34.9
15.3	2.2	33.4	N7A	14.7	3.3	32.6
15.5	2.9	32.3	C8A	15.0	4.2	31.7
16.1	4.1	32.6	N9A	15.9	5.2	32.0
15.4	1.7	36.4	N10A	15.0	2.1	35.3
16.4	5.3	31.8	C1R	16.4	6.1	31.0
16.9	4.9	30.4	C2R	16.9	5.5	29.8
18.3	4.5	30.4	O2R	18.3	5.1	30.0
16.7	6.1	29.6	C3R	16.8	6.6	28.7
17.7	7.1	29.6	O3R	17.9	7.4	28.6
15.4	6.7	30.2	C4R	15.6	7.3	29.2
15.3	6.1	31.6	O5R	15.4	7.0	30.6
14.1	6.4	29.6	C5R	14.3	7.0	28.4
13.5	7.6	29.0	O6R	14.1	8.3	27.8
13.8	7.8	27.4	PA	13.4	8.5	26.4
13.9	6.5	27.0	OP1A	13.2	7.2	25.7
15.0	8.6	27.2	OP2A	14.2	9.3	25.6
12.5	8.6	27.0	OP3	12.2	9.1	27.0
11.9	10.2	27.0	PN	11.2	10.3	26.6
10.5	10.2	26.3	OP1N	10.8	10.2	25.2
12.8	11.2	26.4	OP2N	11.8	11.6	26.8
11.7	10.6	28.5	O6Q	9.9	10.1	27.5
10.4	11.0	29.0	C5Q	10.0	9.5	28.8
8.2	9.3	30.0	O5Q	7.6	10.0	29.4
9.8	9.6	29.8	C4Q	8.6	9.0	29.3
10.1	8.2	29.1	C3Q	8.0	7.9	28.5
10.6	7.2	29.9	O3Q	7.4	6.8	29.3
8.7	7.7	28.5	C2Q	6.9	8.6	27.7
8.9	6.3	28.2	O2Q	5.9	7.6	27.4
7.7	8.1	29.5	C1Q	6.5	9.7	28.8
6.3	8.1	28.8	N1N	5.9	11.0	28.3
5.9	7.1	27.9	C2N	4.8	11.5	28.9
4.8	7.3	27.1	C3N	4.3	12.7	28.5
3.9	8.4	27.3	C4N	4.8	13.5	27.5
4.4	9.3	28.3	C5N	6.0	12.9	26.9
5.5	8.9	28.9	C6N	6.5	11.7	27.2
4.4	6.3	26.0	C7N	3.0	13.4	29.2
3.1	6.4	25.6	N2N	2.6	14.5	28.9
5.2	5.4	25.7	O1N	2.3	12.6	30.1

orthorhombic LADH-H_2NADH-MPD complex				triclinic LADH-H_2NADH-DACA complex			
MPD				DACA			
	X	*Y*	*Z*		*X*	*Y*	*Z*
Zn_{cat}	4.1	12.7	22.8	Zn_{cat}	4.8	13.1	23.3
C1	−0.5	12.1	26.6	O1	3.5	12.4	24.9
C2	0.1	10.8	26.8	C1	2.6	11.4	24.8
O2	1.6	10.8	26.6	C2	1.6	11.2	25.8
C3	−0.4	9.7	25.9	C3	0.7	10.1	25.7
C4	−0.4	8.3	26.8	C4	−0.3	9.9	26.7
C5	0.3	9.0	28.0	C5	−0.3	10.7	27.8
C6	−1.7	7.7	27.3	C6	−1.3	10.5	28.9
O4	0.4	7.3	26.3	C7	−2.2	9.5	28.7
				C8	−2.2	8.6	27.5
				C9	−1.2	8.8	26.5
				N	−3.2	9.2	29.7
				C10	−3.2	10.1	30.9
				C11	−4.2	8.1	29.6

[a] The triclinic coordinates have been transformed into the orthorhombic coordinate system. α carbon atoms in the coenzyme binding domains of the two structures are superimposed by a least-squares fit and the matrix obtained is applied to the triclinic coordinate set for the ligands (subunit 2).

H_2NADH–MPD complex.

A comparison between the LADH–H_2NADH–MPD complex and the native enzyme has not revealed any great differences in the water binding pattern of the cleft between the domains or in the substrate binding site, although the pH of the solution in which the complex was formed is 1 pH unit higher than the pH for the native protein. Minor shifts in the water coordinates are found in the vicinity of the pyro-

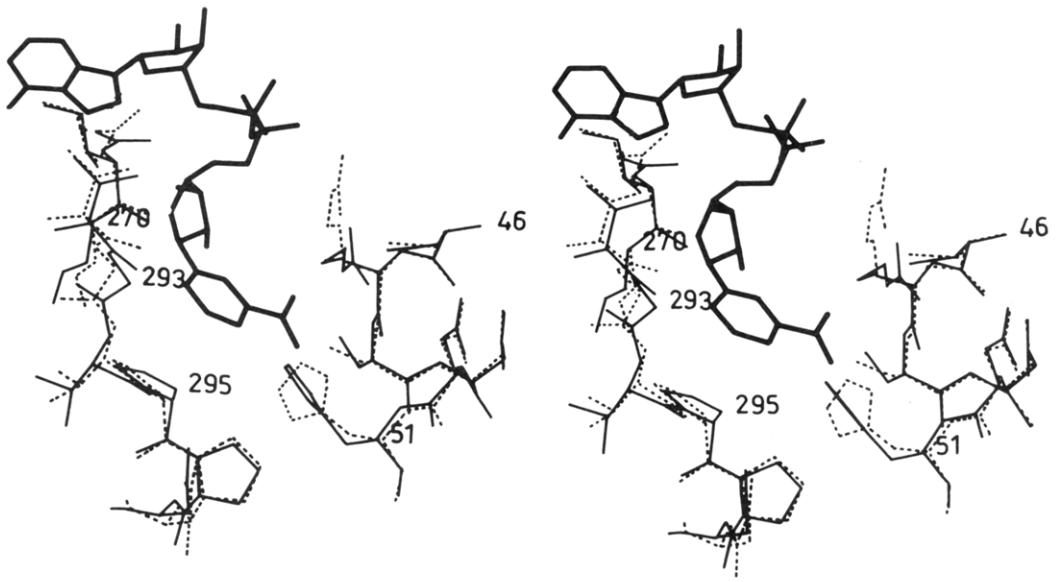

FIGURE 4: Stereo diagram illustrating the position of the H_2NADH molecule within the cleft between domains in the orthorhombic LADH. The local structural changes that occur upon H_2NADH binding in this part of the protein are indicated. Thin, solid lines = unliganded enzyme; dashed lines = the enzyme complex; thick, solid lines = the coenzyme analogue. Residues 293–296 are part of a loop that undergoes considerable changes in the triclinic substrate complex. The peptide segment 46–51 is part of a helix that covers the active site zinc sphere.

Table III: Position of Water Molecules in the Coenzyme Binding Cleft and the Active Site Region of the Orthorhombic LADH-H_2NADH-MPD Complex[a]

	coordinates			atoms within 2.7–3.2-Å distance to water	
	X	*Y*	*Z*		
H_2O 1	−3.5	1.2	18.2	O52 O57 H_2O 2	interior; close to the tetrahydronicotinamide ring
H_2O 2	−5.8	−0.7	19.0	O59 H_2O 1	connects H_2O 1 to the surface of the subunit
H_2O 3	4.8	13.0	17.0	O44 N67 N68	interior; distal to active site zinc atom (Figure 5); located in difference electron density in $F_{obsd} - F_{calcd}$ Fourier maps also in the triclinic complex
H_2O 4	2.4	14.7	28.0	OG178 N319 H_2O 6	interior; in a position where the tetrahydronicotinamide ring binds in the triclinic substrate complex
H_2O 5	9.6	10.4	23.8	OP1N H_2NADH H_2O 11	part of the water bridge in the region between domains
H_2O 6	2.9	13.4	30.4	O317 O292 H_2O 4	interior; in a position where the tetrahydronicotinamide ring binds in the triclinic substrate complex
H_2O 7	3.8	16.3	32.3	OG182 O317 H_2O 6	interior; deep inside the active site region
H_2O 8	2.9	12.2	24.3	OG48 MPD	fourth ligand to active site zinc atom with a bond distance of 2 Å
H_2O 9	12.7	10.5	18.8	O45 O368 N369	interior; not far from the catalytic zinc sphere
H_2O 10	6.4	13.4	26.1	H_2O 11	part of the water bridge located between domains; position close to active site zinc ligand SG174
H_2O 11	8.5	12.7	24.1	SG46 NEH2 369 H_2O 10 H_2O 5	link between active site zinc ligand SG46, H_2NADH, and catalytic domain
H_2O 12	12.5	15.7	23.1	NEH1 369	link between domains

[a] The water sites were determined from difference Fourier maps with the amplitudes $F_{obsd} - F_{calcd}$. Peak heights and the possibilities for assumed water molecules to form hydrogen bonds to neighboring atoms are criteria used to select these positions. Coordinates are given in angstrom units along the orthorhombic cell axes.

phosphate bridge. Electron density, interpreted as a water in the fourth ligand position to the active site metal atom, is clearly identified in the maps. Water sites introduced in the complex structure are illustrated in Figure 3C, and Table III lists the environment of water positions present in the active site region of the LADH-H_2NADH-MPD complex. The quality of the electron density maps gave us confidence in our data, and we want to stress that we have been restrictive in our assignment of possible water positions in this complex.

In spite of the fact that the H_2NADH molecule occupies a large part of the cleft separating the domains of the subunit, there is still space left where electron density is observed and

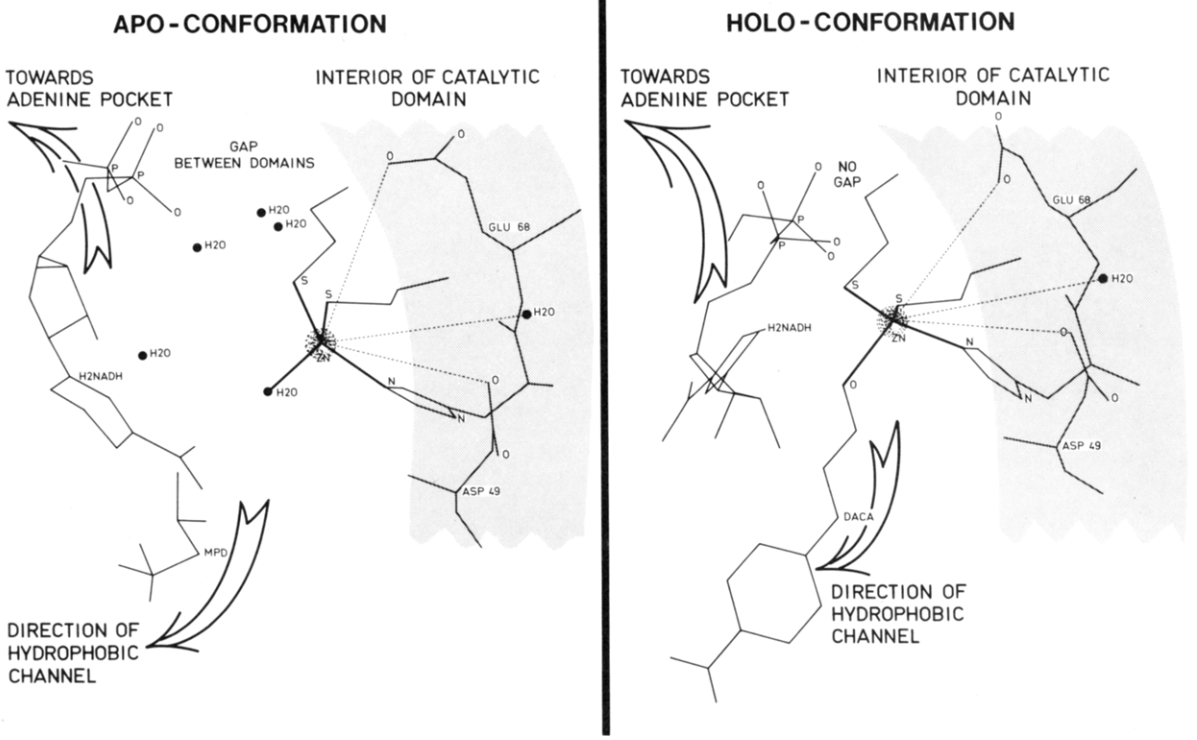

FIGURE 5: Schematic drawing showing the nearest neighbors to the active site zinc atom of the orthorhombic LADH–H_2NADH–MPD complex (left) and the triclinic LADH–H_2NADH–DACA complex (right). The dashed lines are not bonds; they only demonstrate the presence of two carboxylate groups and one water molecule hidden inside the domain without direct contact to the surface of the protein. The distances between these groups and the center of the metal atom correspond to 5.5–6 Å. The C4, C5, and C6 atoms of the tetrahydronicotinamide ring are at van der Waals distances to the metal center and the cysteine ligands in the holo conformation.

these peaks have been interpreted as water molecules. They form links between the coenzyme analogue and the side chains of the catalytic domain. One contact across the cleft is made via the pyrophosphate bridge, water, and the sulfur ligands to the active site zinc (Table III). We have combined our interpretation with the results from accessibility calculations (Lee & Richards, 1971) on the LADH complexes described in this work. Such calculations are reported in Table IV. Column 3 gives the accessible surface area expressed in square angstroms for H_2NADH in the orthorhombic structure, where the coenzyme binding cleft is open and wide. It is clearly seen that three of the phosphate oxygens are accessible and one less so. This result supports our interpretation that the positions where we observe electron density in the cleft between the phosphates and the catalytic domain could be assigned as water molecules.

The active site zinc atom is four coordinated in the LADH–H_2NADH–MPD complex similar to the native enzyme (Eklund et al., 1976). It is important to recall that the active center is situated 20 Å from the surface of the subunit, at a point where two ligand binding channels meet (Figure 1). The zinc ligands S46–S174–N67 are closest to amino acids located in the catalytic domain, whereas the bond direction for the fourth ligand to zinc is toward the substrate binding channel into which metal-bound water protrudes. The inner coordination sphere of zinc is surrounded by several hydrophilic groups within a radius of 7.5 Å. The chemical environment in the vicinity of the active site zinc in the LADH–H_2NADH–MPD complex is schematically presented in Figure 5 (left). This picture also indicates that the space between domains in the apo conformation of LADH is large enough to accommodate the pyrophosphate bridge of a coenzyme together with water or perhaps small ions.

Table IV: List of Atoms with Accessible Surface Area Equal to or Greater Than One Square Angstrom

atom name	H_2NADH in triclinic LADH (Å²) subunit 1	H_2NADH in triclinic LADH (Å²) subunit 2	H_2NADH in orthorhombic LADH (Å²)
N1A	3	5	4
N7A	6	8	6
C8A	19	12	20
N10A	14	15	17
C2R	11	10	10
O2R	5	8	7
C3R	2	7	4
C5R	5	5	10
PA	0	0	2
OP1A	1	1	8
OP2A	0	0	5
OP3	0	0	1
PN	0	0	2
OP1N	0	0	6
OP2N	0	0	2
O2Q	0	0	13
C2N	0	0	2
C4N	0	0	1
C5N	0	0	13
C6N	0	0	5

(c) Structural Changes in the Apo Conformation Induced by the H_2NADH Binding. Local structural changes in the enzyme are observed upon H_2NADH binding, but no concerted movements propagating through a whole domain due to ligand interactions can be detected in this complex. Certain surface side chains obtain fixed orientations because they participate in coenzyme analogue binding. Structural changes also occur in the interior of the coenzyme and substrate binding sites where residues reorient slightly in the presence of

Scheme I: Differences in the Interactions between Ser-48 and His-51 and Groups in the Active Site for Three LADH Structures[a]

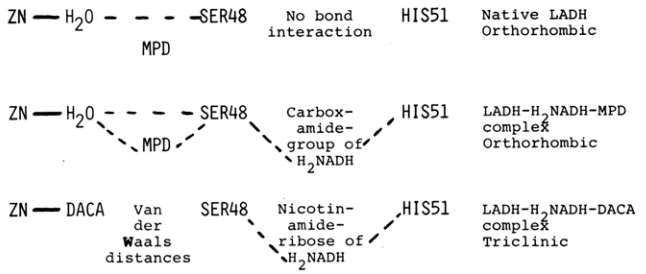

[a] Dashed lines indicate possible hydrogen-bond interactions.

H_2NADH. The most striking example is the changed orientation of His-51. The presence of the tetrahydronicotinamide ring in the vicinity of this residue forces the histidine side chain to rotate around its Cα–Cβ bond. In Figure 3C it is clearly seen that the carboxamide group of H_2NADH forms contacts with His-51 and Ser-48. Scheme I presents the relationship between His-51, Ser-48, and zinc-bound water derived from the refined native enzyme structure (A. Jones, unpublished results) and the new interaction pattern found for these groups in the coenzyme analogue complex. In Figure 4, the comparison between the native structure and the LADH–H_2NADH–MPD complex is made for a region where particularly large conformational changes occur (Eklund et al., 1981) in triclinic LADH complexes.

(d) Binding of H_2NADH and DACA to the Triclinic Holoenzyme Conformation. The holoenzyme structure has been investigated and the conformation differences between the apoenzyme and the LADH–NADH–Me_2SO complex are extensively described by Eklund et al. (1981). The conformation transition involves a rotation of the two catalytic domains with respect to the central core of the dimer, the tightly connected coenzyme binding domains. The rotation axis is located along the pleated sheet structure βI in the catalytic domain and is indicated in the schematic drawing of the LADH molecule in Figure 1.

In the triclinic substrate complex each subunit binds one H_2NADH molecule. The occupancies, judged from the peak heights, are similar, and the difference electron densities are shown in Figure 6. The models of the two analogue molecules fitted to these difference densities are indistinguishable from the NADH model presented by Eklund et al. (H. Eklund, C.-I. Brändén, J.-P. Samama, and T. A. Jones, unpublished experiments). Within the limits of errors for the present triclinic model, the interactions between H_2NADH and the protein are similar for the two subunits. Since the binding of the analogue in the substrate complex is comparable to that of NADH bound to the LADH–NADH–Me_2SO complex, the coenzyme–protein interactions described by Eklund et al. (H. Eklund, C.-I. Brändén, J.-P. Samama, and T. A. Jones, unpublished experiments) fully explain the interactions between H_2NADH and LADH found in this work. This result establishes that the analogue used behaves as a natural coenzyme with respect to its binding interactions to the enzyme and can therefore be regarded as a suitable model to describe the orientation of the coenzyme in a ternary aldehyde complex. Table II lists the coordinates for H_2NADH (in subunit 2) transformed to the orthorhombic coordinate system. An overall view of the relationship between the H_2NADH molecule and the active site residues in the triclinic protein model is shown in Figure 7A; charged or polar interactions between atoms of the analogue and the protein are indicated. The

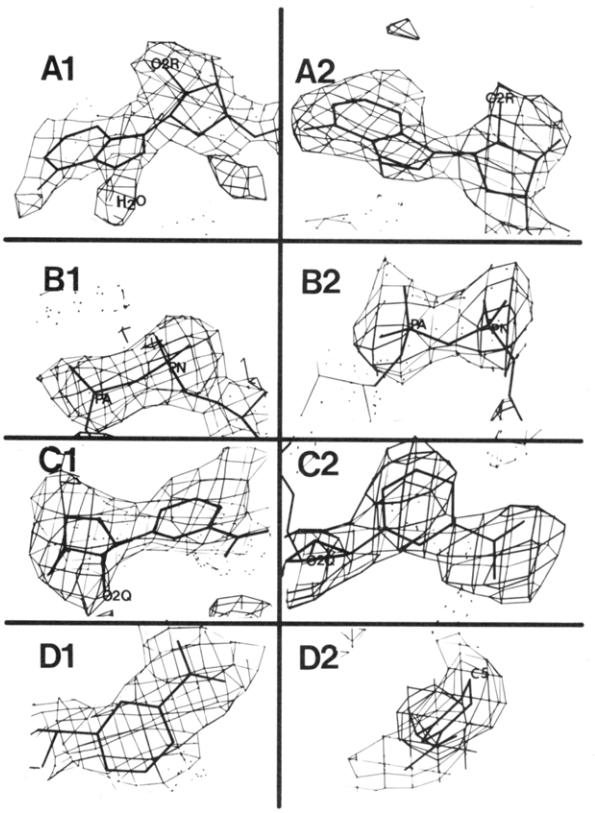

FIGURE 6: Parts of the difference electron density map F_{obsd}(LADH–H_2NADH–DACA) – F_{calcd}(LADH–holoprotein) of the 2.9-Å resolution triclinic complex. The phase angles are derived from the refined triclinic enzyme model determined to 2.9-Å resolution. Segments A1–D1 correspond to the H_2NADH model superimposed on the difference density in subunit 1 and segments A2–D2 for subunit 2.

structure is oriented such that a comparison with Figure 3C is convenient. From this comparison it is evident that the Arg-369 is in direct contact with the pyrophosphate bridge in the triclinic complex, in contrast to the orthorhombic. Ser-48 and His-51 make close interactions with the second ribose (Figure 8), giving a different interaction pattern for these two residues compared with that of the LADH–H_2NADH–MPD complex and the native structure. Scheme I illustrates these differences.

The binding of H_2NADH to the holo conformation is accompanied by displacement of several water molecules. The position of the tetrahydronicotinamide ring in the LADH–H_2NADH–DACA complex corresponds to water binding sites in the LADH–H_2NADH–MPD complex, as illustrated in Figure 8. Furthermore, due to the conformational change in the protein the catalytic domain is brought too close to the pyrophsphate bridge to allow space for the binding of water molecules. Accessibility calculations for H_2NADH bound to the triclinic structure substantiate this fact. Columns 1 and 2 in Table IV show that the accessible surface areas for the pyrophosphate oxygens are zero. The schematic representation in Figure 5 (right) illustrates that an entirely water free environment has been created at the site where the hydrid transfer reaction takes place.

The complexes LADH–NADH–DACA and LADH–H_2NADH–DACA have been crystallized at pH 9.5 where the stability of a transient intermediate is maximal (Dunn & Hutchison, 1973; Dunn et al., 1975). The visible and ultraviolet spectra of single crystals were recorded at the same pH. The optical density vs. wavelength is plotted in Figure 9 and shows the absorption bands at 325 and 464 nm that are

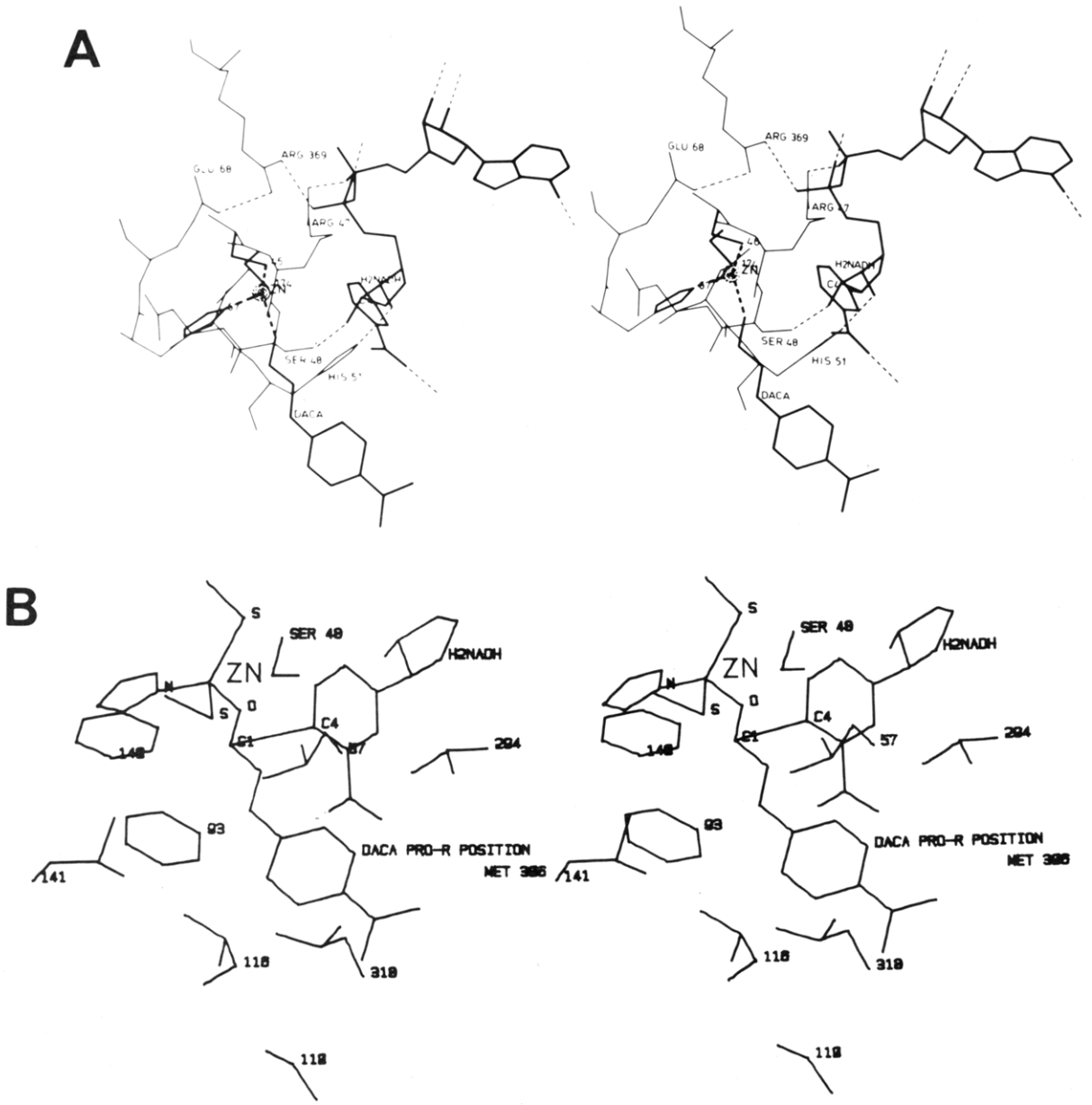

FIGURE 7: Binding of H_2NADH and DACA to the triclinic holo conformation of LADH. (A) The coenzyme analogue molecule, active site residues, and the substrate. Dashed lines indicate possible hydrogen bonds and salt bridges between the H_2NADH and the protein. (B) The DACA molecule in the hydrophobic binding channel. The residues displayed or indicated with text are leucines-57, -116, and -141, phenylalanines-93, -110, and -140, isoleucine-318, and methionine-306 from the other subunit. This orientation of the substrate is derived from model building and corresponds to a *pro-R* stereospecific position.

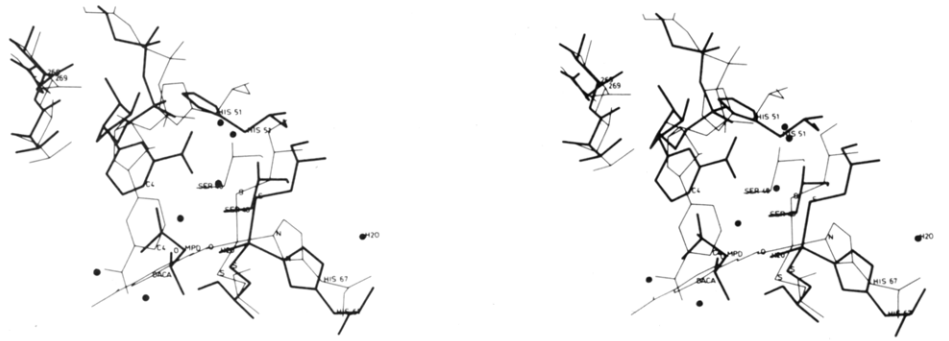

FIGURE 8: Stereo diagram illustrating the position of the tetrahydronicotinamide ring of H_2NADH, the DACA substrate, and the MPD molecule in relation to the active site zinc atom and the side chains Ser-48 and His-51. The two structures are superimposed (thick lines = orthorhombic complex, thin lines = triclinic complex). The matrix used for the transformation of the triclinic coordinates to an orthorhombic coordinate system is based on the α carbon atom positions in the 12-membered β sheet of the two coenzyme binding domains. This core structure of the enzyme has the smallest differences in intermolecular vector lengths between pairs of chemically identical α carbons (Eklund et al., 1981). The comparison shows that the productive position of the H_2NADH in the aldehyde complex coincides with water positions (black dots) in the abortive alcohol complex.

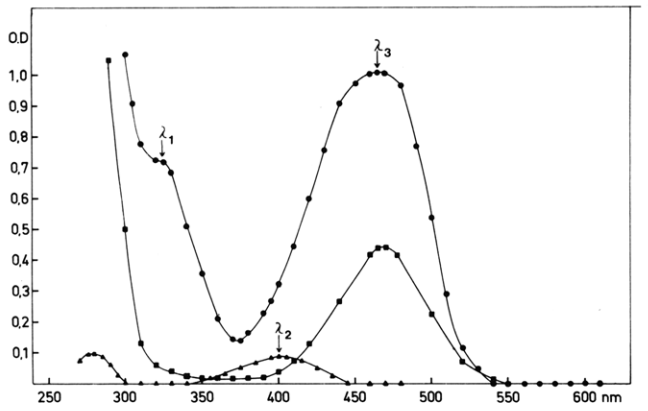

FIGURE 9: Absorption spectrum of a single crystal of the triclinic LADH–H_2NADH–DACA complex (■) compared with that of a LADH–NADH–DACA crystal (●). The transmission values from the recorder have been recalculated to optical density units. The spectrum of the suspending medium around the crystals (▲) is obtained by subtracting the absorption of the quartz glass. Crystal thickness and orientation in the unpolarized beam are different in the two samples. λ_3 denotes the absorption maximum of zinc-bound DACA, λ_2 is the absorption maximum of free DACA in solution, and λ_1 is the characteristic shoulder due to enzyme-bound NADH.

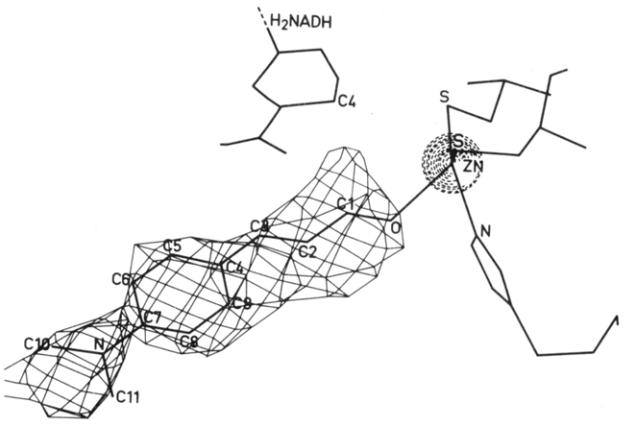

FIGURE 10: Model of the DACA substrate superimposed on an $F_{obsd} - F_{calcd}$ Fourier map, where the contribution for the coenzyme analogue coordinates has been introduced to a structure factor calculation and selected active site residues were subtracted.

characteristic for enzyme-bound NADH and enzyme-bound DACA, respectively. LADH–H_2NADH–DACA crystals exhibit the characteristic 468-nm absorption band for bound aldehyde and consistently lack the 325-nm shoulder of NADH. The spectrum of the diluted mother liquor surrounding the crystals shows the absorption maximum of free aldehyde at 398 nm. These qualitative spectral data on the single crystals show that the substrate complex described by Dunn et al. (1975) is actually present in the crystals used for the X-ray experiments. Since crystal size as well as the crystal orientation during spectral recording has been different from sample to sample, the concentration of ligand within the crystals is unknown.

The binding of DACA determined from the X-ray data was interpreted from $F_{obsd} - F_{calcd}$ Fourier maps by using calculated phases for which the contributions from the H_2NADH coordinates were added and selected active site residues were omitted in the structure factor calculation. Electron density is observed in the substrate binding site in both subunits. The density extends from the active site zinc atom through the hydrophobic substrate channel (Figure 7B) in the direction of Met-306 from the other subunit. When the distance between the aldehyde oxygen and the zinc atom is approximately 2 Å, the whole substrate model is covered by density (Figure 10). We conclude that the substrate oxygen is directly liganded to zinc and that zinc-bound water is exchanged. The coordination geometry remains roughly tetrahedral, and there is no indication in our electron density maps of a fifth ligand to the metal atom. Indirect coordination, via metal-bound water, would position the substrate model far out of the density and cause severe close contacts to residues lining the substrate binding pocket.

In our model building of the aldehyde substrate we make the assumption that the bound molecule is planar, in accordance with the interpretation of the spectral characteristics for the chromophore. If the planar system is built into density so that the maximal best fit (Figure 10) is obtained, ideal van der Waals distances are observed between protein atoms and the substrate molecule. The carbon atom C1, which would receive the reacting hydrogen atom, is at a distance 4 Å from the C4 atom of the tetrahydronicotinamide ring, and the angle between the normals of the substrate plane and the ring plane is 70°. This orientation of DACA is illustrated in Figures 7A and 8 and represents a mode of binding where direct hydride transfer cannot take place. The DACA model can be rotated within the density 30–40° from the previous position and maintain acceptable van der Waals interaction distances between the substrate and groups in the binding site. This position of the model orients the substrate for *pro-R* stereospecificity, and the distance between the hydrogen atom at C4 and C1 becomes 3.6 Å. The result of this model building is presented in Figure 7B. The stereospecificity for the DACA substrate has not been determined; it would be interesting to obtain data for the stereospecificity for this particular substrate as it is a widely used compound in LADH studies.

Minor structural changes occur in the substrate binding pocket upon DACA binding. Compared to the LADH–NADH–Me_2SO complex, Leu-116 and Met-306 clearly have changed their positions. These side chain movements avoid unfavorable van der Waals contacts with the bulky phenyl ring and the dimethylamino group of the substrate molecule. Transformed coordinates for the DACA molecule, as it is represented in Figures 7A and 8 for subunit 2, are listed in Table II.

The active site zinc atom clearly has a different environment in the triclinic substrate complex as compared to the orthorhombic H_2NADH–MPD complex. The zinc-bound water is exchanged, and second-sphere water molecules in the cleft between domains have been displaced. However, the "distal" side of the zinc sphere is similar in both enzyme conformations. The buried charged residues, Glu-68 and Asp-49, have approximately the same distances to the metal center [Figure 5 (right)].

(*e*) *Comparison between the H_2NADH Models.* The similarities and differences between the conformations of H_2NADH bound to the apo and holo structures of LADH are most clearly demonstrated when the two coenzyme analogue models are superimposed and the distance differences are calculated between each atom. Table V shows that the distance differences are 0.1–0.5 Å for the adenosine part of the molecule. This agrees with the observations made earlier that NADH and other coenzyme analogues (Samama et al., 1977, 1981) bound to LADH have similar conformations in the AMP portion regardless of how the rest of the molecule is folded. The distance differences increase to 3–8 Å for atoms in the tetrahydronicotinamide ring. Figure 11A illustrates the result of the superposition based on the coordinates in Tables II and V. H_2NADH bound to the apoenzyme complex has a less extended conformation than H_2NADH in the holo-

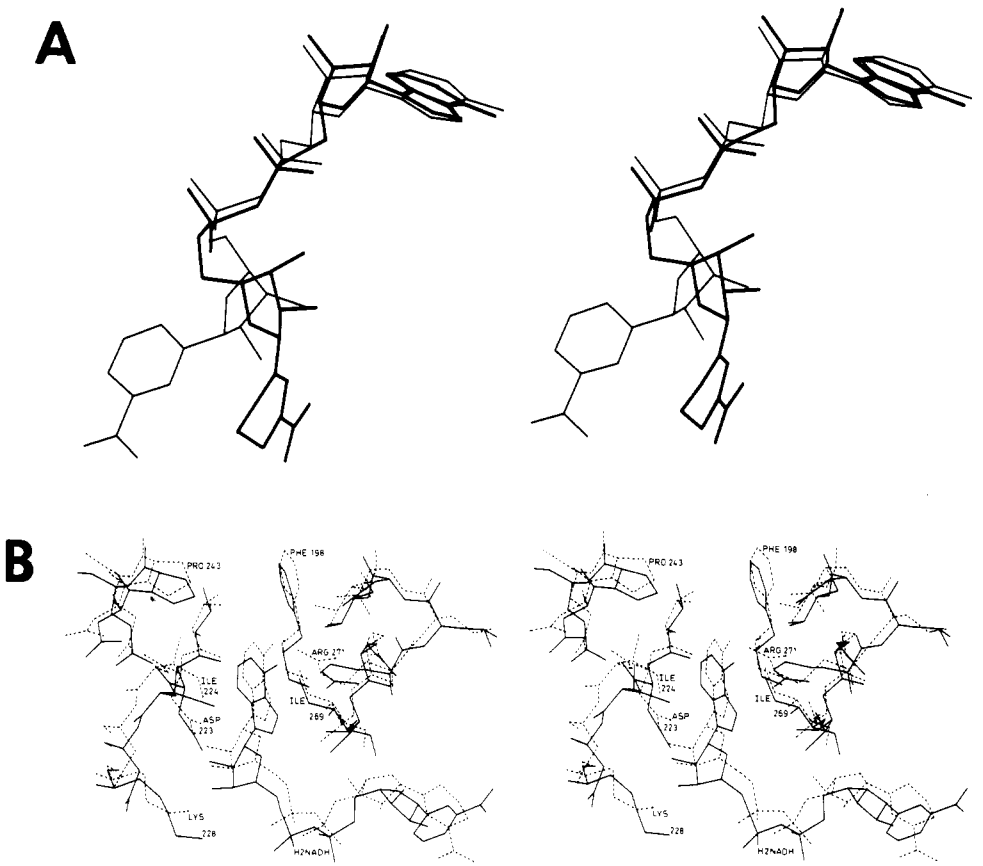

FIGURE 11: Stereo diagram that illustrates the similarities and differences in the conformation of H_2NADH models. (A) Data from Tables II and V. Thick lines = H_2NADH in the apo conformation, thin lines = H_2NADH in the holo conformation of LADH. (B) Comparison made with respect to the protein structure (subunit 2). Solid lines = transformed triclinic coordinates; dashed lines = orthorhombic complex.

enzyme complex. This dissimilarity originates from differences in conformational angles θ_N and χ_N (see Table I).

Another way of comparing the two H_2NADH models is to study them in relation to the protein structure. Equivalent α carbon atom positions in the coenzyme binding domains except residues 292–298 (Eklund et al., 1981) were superimposed. The result of such a comparison is illustrated in Figure 11B. A translation in the H_2NADH position can be observed that reflects the effect of the gross conformational change in the enzyme. A detailed presentation of this effect will be published elsewhere.

Discussion

This investigation deals with two important aspects of the catalytic cycle of horse liver alcohol dehydrogenase: (1) binding of substrate molecules in the active site and their interactions with the catalytic zinc atom; (2) the nature of the effector role played by the coenzyme molecule both in the correct positioning of the substrate and in the induction of a conformational transition in the enzyme.

The occurrence of two crystal forms from a solution containing enzyme, H_2NADH, DACA, and the precipitating agent MPD may be explained by the simplified equilibrium scheme

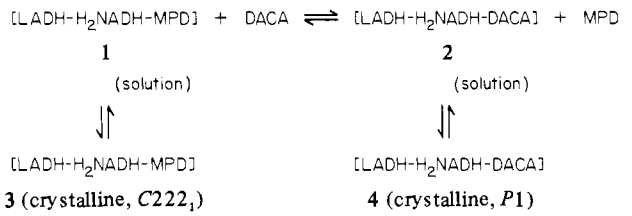

The solvent 2-methyl-2,4-pentanediol is a weakly binding substrate (Plapp et al., 1978) with a K_m of about 0.7 M. There is obviously competition between DACA and MPD leading to the formation of considerable amounts of complex **1** when the concentration of DACA is low (experiment a under Materials and Methods). Since the solubility of complex **1** is lower than that of complex **2**, orthorhombic crystals **3** start to form at a 12% solvent concentration. Depending on the amount of DACA present, the concentration of the ternary complex **2** can be increased in the equilibrium mixture until eventually almost all the protein is complexed in this form and crystallization occurs as soon as the MPD concentration exceeds 17% (experiment b under Materials and Methods).

The important event in the transition of the complex LADH–H_2NADH–MPD to the complex LADH–H_2NADH–DACA is the gross structural transition in the protein (Eklund et al., 1981). Thus the system described above consists of at least two species with different conformational states. It is obvious that both coenzyme and substrate play an important role in the formation of the triclinic aldehyde complex. The use of H_2NADH instead of NADH was necessitated by the requirement for prolonged stability of the complexes during crystallization and X-ray experiments on a time scale of months. The LADH–H_2NADH–DACA complex is extremely stable and does not break down to give products, whereas the complex LADH–NADH–DACA turns over slowly. The only structural change upon hydrogenation of the 1,4-dihydronicotinamide ring is a 0.64-Å deviation from planarity in the C5N position (Hope, 1969). We observe differences in the crystal forms when we precipitate enzyme–NADH or –H_2NADH complexes with high concentrations of MPD. The LADH–NADH complex crystals used for the microspectro-

Table V: List of Coordinates and Distance Differences, in Angstrom Units, between 1,4,5,6-Tetrahydronicotinamide Adenine Dinucleotide (H_2NADH) Bound in Orthorhombic and Triclinic LADH[a]

transformed triclinic coordinates			atom	distance
X	Y	Z	name	differences
16.6	3.5	36.7	N1A	0.4
17.0	4.7	36.2	C2A	0.4
16.8	5.1	34.9	N3A	0.2
16.2	4.2	34.1	C4A	0.1
15.8	3.0	34.5	C5A	0.1
16.0	2.6	35.9	C6A	0.3
15.2	2.3	33.4	N7A	0.1
15.3	3.2	32.4	C8A	0.4
15.9	4.3	32.8	N9A	0.3
15.6	1.4	36.4	N10A	0.4
16.4	5.5	32.0	C1R	0.3
16.8	5.1	30.6	C2R	0.3
18.1	4.6	30.6	O2R	0.3
16.7	6.5	29.9	C3R	0.5
17.8	7.3	30.0	O3R	0.5
15.5	7.1	30.5	C4R	0.5
15.3	6.4	31.8	O5R	0.4
14.2	7.0	29.7	C5R	0.6
14.4	7.9	28.6	O6R	1.0
13.8	7.5	27.2	PA	0.4
13.6	6.1	27.0	OP1A	0.5
14.7	8.0	26.1	OP1A	1.3
12.5	8.3	27.3	OP3	0.4
12.0	9.7	26.7	PN	0.6
11.3	9.5	25.4	OP1N	1.4
13.1	10.7	26.6	OP2N	0.6
10.9	10.2	27.8	O6Q	1.1
11.1	9.9	29.2	C5Q	1.3
8.9	10.1	30.3	O5Q	1.1
9.9	9.1	29.7	C4Q	0.5
9.1	8.3	28.8	C3Q	1.0
8.7	7.0	29.2	O3Q	2.0
7.9	9.2	28.4	C2Q	1.7
6.8	8.4	28.2	O2Q	3.0
7.7	10.0	29.7	C1Q	2.0
7.2	11.4	29.1	N1N	3.4
5.9	12.0	29.5	C2N	5.1
5.5	13.1	28.9	C3N	6.1
6.3	13.8	28.0	C4N	6.0
7.5	13.2	27.7	C5N	5.0
8.0	12.0	28.2	C6N	4.0
4.1	13.8	29.2	C7N	8.2
3.4	13.2	30.2	N2N	8.2
3.8	14.8	28.6	O1N	9.9

[a] The orthorhombic coordinates are listed in Table II. The transformed triclinic coordinates were obtained by using a least-squares procedure that determines a rotation matrix that allows the AMP part of the triclinic structure to coincide with the AMP moiety in the orthorhombic structure.

photometric measurements in this work are triclinic in contrast to the orthorhombic LADH–H_2NADH complex described. Similarly, the NADH complex with MPD analyzed by Plapp et al. (1978) formed triclinic crystals. Although the mode of binding of MPD to the triclinic holo structure could not be definitely determined by Plapp from the 4.5-Å isomorphous difference Fourier maps, it is clear that the trigger mechanism for the conformational transition in LADH is a sensitive and complex process.

Binding of Substrate in the Active Site. The present study has provided the opportunity of comparing the mode of binding of a substrate molecule in an "abortive" complex, LADH–H_2NADH–MPD, where the protein has retained its native conformation, and a "productive" aldehyde complex, LADH–H_2NADH–DACA. The important difference is obvious. In the abortive complex the substrate is bound indirectly via the zinc-bound water molecule, whereas in the productive complex the substrate coordinates directly to the catalytic metal ion (Figure 5). In the productive aldehyde complex, the spectral properties of our crystals of LADH–H_2NADH–DACA are similar to those of the complex in solution described by Dunn et al. (1975). Our data provide the final proof for the conclusions drawn from spectroscopic measurements in solution. Dunn & Hutchison (1973) interpreted the 464-nm chromophore as a result of direct coordination of the aldehyde to zinc in LADH. Model compounds of metal complexes with DACA derivatives (Angelis et al., 1977) showed a corresponding red shift, the magnitude of which was dependent on the nature of the metal in the model complex. Furthermore, Dietrich et al. (1979) have shown that zinc-depleted LADH does not have the ability to form the transient complex. In the cobalt-substituted enzyme the chromophore is formed with an even larger red shift (λ_{max} = 478 nm) than in the zinc–enzyme. From our single crystal spectra it is evident that we have analyzed the same crystalline complex as described in solution. This is especially important as it has been argued (Sloan et al., 1975) that differences in substrate binding might exist between crystalline complexes and LADH complexes in solution states.

An Effector Role of the Coenzyme. The use of DACA as a substrate not only has given insight into the interactions between the catalytic site and the substrate but also has provided an opportunity to investigate the role of the coenzyme. The formation of a stable transient with NADH or H_2NADH has revealed details about the time course of the catalytic cycle and thereby given evidence that the coenzyme does not exclusively act as a cosubstrate but also acts as a noncovalent effector (Dunn & Hutchison, 1973). The 464-nm chromophore cannot form unless the cofactor has prepared the enzyme protein to receive the substrate. From spectroscopic measurements on the cobalt-substituted LADH (Maret et al., 1979) it was directly observed that the modulator process involves changes within the coordination sphere at the active site metal. The "blue hybrid", where only the catalytic zinc atom has been exchanged by cobalt, shows changes in the visible spectrum upon binary complex formation with NADH or H_2NADH. Subsequent binding of DACA shifts the spectrum further, and the interpretation is that a successive distortion of the coordination sphere of the cobalt occurs. The zinc–enzyme and the blue hybrid are closely related (Dietrich et al., 1979; G. Schneider, H. Eklund, E. Cedergren-Zeppezauer, and M. Zeppezauer, unpublished experiments), and our present results on the binding of H_2NADH and DACA are therefore highly relevant to the binding studies, made for the same ligands, to the cobalt species. Structural information about the geometry of the metal atom in a binary crystalline LADH–NADH complex is not available. Crystals grown without any precipitating alcohol present (Yonetani & Theorell, 1963; Zeppezauer et al., 1967) are monoclinic, which implicates a structural transition in the protein (Samama, 1979) involving rearrangements in the neighborhood of the active site metal center similar to those observed in triclinic complexes. The changes observed in the cobalt spectrum upon NADH or H_2NADH binding might partially be due to displacement of second sphere water molecules. The further shift in the visible spectrum when DACA is added (Dietrich, 1980; Dunn et al., 1982) clearly reflects the modification of the inner coordination sphere of the metal, since the DACA substrate is directly liganded to zinc in the ternary complex. However, the geometry of zinc in the LADH–H_2NADH–DACA complex is tetrahedral with the same protein ligands as in unliganded zinc- (Eklund et al., 1976) and cobalt-substituted

enzymes (G. Schneider, H. Eklund, E. Cedergren-Zeppezauer, and M. Zeppezauer, unpublished experiments). Thus neither a change in coordination number nor a large change in coordination geometry is observed at the present level of resolution. The modulator action of the coenzyme on the conformational change of the protein obviously can be affected. In the LADH–H_2NADH–MPD complex the conformational change has been inhibited, which demonstrates that the nature of the fourth ligand to the active site metal is of importance for this process.

Acknowledgments

We appreciate discussions with Professors C.-I. Brändén, J.-F. Biellmann, M. F. Dunn, and M. Zeppezauer. We thank Ing. G. Lomakka and P. Issler at the Karolinska Institute, Stockholm, who introduced E.C.-Z. in the use of the Zeiss UMSP1 microspectrophotometer. We thank Dr. T. A. Jones for access to phase angles during the course of the refinement of the LADH structures and Anita Rogelius for typing the manuscript.

References

Abdallah, M. A., Biellmann, J.-F., Nordström, B., & Brändén, C.-I. (1975) *Eur. J. Biochem. 50*, 475–481.

Angelis, C. T., Dunn, M. F., Muchmore, D. C., & Wing, R. M. (1977) *Biochemistry 16*, 2922–2928.

Biellmann, J.-F., & Jung, M. J. (1971) *Eur. J. Biochem. 19*, 130–134.

Bignetti, E., Rossi, G. L., & Zeppezauer, E. (1979) *FEBS Lett. 100*, 17–22.

Dietrich, H. (1980) Ph.D. Thesis, Universität des Saarlandes, Saarbrücken, Federal Republic of Germany.

Dietrich, H., Maret, W., Wallén, L., & Zeppezauer, M. (1979) *Eur. J. Biochem. 100*, 267–270.

Dunn, M. F., & Hutchison, J. S. (1973) *Biochemistry 12*, 4882–4892.

Dunn, M. F., Biellmann, J.-F., & Branlant, G. (1975) *Biochemistry 14*, 3176–3182.

Dunn, M. F., Dietrich, H., MacGibbon, A. K. H., Koerber, S. C., & Zeppezauer, M. (1982) *Biochemistry 21*, 354–363.

Eklund, H., Nordstöm, B., Zeppezauer, E., Söderlund, G., Ohlsson, I., Boiwe, T., Söderberg, B.-O., Tapia, O., Brändén, C.-I., & Åkesson, Å (1976) *J. Mol. Biol. 102*, 27–57.

Eklund, H., Samama, J.-P., Wallén, L., Brändén, C.-I., Åkesson, Å., & Jones, T. A. (1981) *J. Mol. Biol. 146*, 561–587.

Hope, H. (1969) *Acta Crystallogr., Sect. B B25*, 78–87.

Jones, T. A. (1978) *J. Appl. Crystallogr. 11*, 268–272.

Jones, T. A. (1982) *Computational Crystallography* (Sayre, D., Ed.) pp 303–317, Oxford University Press, New York.

Lee, B., & Richards, F. M. (1971) *J. Mol. Biol. 55*, 379–400.

Maret, W., Andersson, I., Dietrich, H., Schneider-Bernlöhr, H., Einarsson, R., & Zeppezauer, M. (1979) *Eur. J. Biochem. 98*, 501–512.

Nordström, B., & Brändén, C.-I. (1975) *Structure and Conformation of Nucleic Acids and Protein-Nucleic Acid Interactions* (Sundaralingam, M., & Raou, S. T., Eds.) pp 387–395, University Park Press, Baltimore, MD.

Plapp, B. V., Eklund, H., & Brändén, C.-I. (1978) *J. Mol. Biol. 122*, 23–32.

Samama, J.-P. (1979) Ph.D. Thesis, *l'*Université Louis Pasteur de Strasbourg, Strasbourg, France.

Samama, J.-P., Zeppezauer, E., Biellmann, J.-F., & Brändén, C.-I. (1977) *Eur. J. Biochem. 81*, 403–409.

Samama, J.-P., Wrixon, A. D., & Biellmann, J.-F. (1981) *Eur. J. Biochem. 118*, 479–486.

Sloan, D. L., Maitland-Young, J., & Mildvan, A. S. (1975) *Biochemistry 14*, 1998–2008.

Sundaralingam, M. (1975) *Structure and Conformation of Nucleic Acids and Protein-Nucleic Acid Interactions* (Sundaralingam, M., & Raou, S. T., Eds.) p 488, University Park Press, Baltimore, MD.

Yonetani, T., & Theorell, H. (1963) *Arch. Biochem. Biophys. 100*, 554–556.

Zeppezauer, E., Söderberg, B.-O., Brändén, C.-I., Åkesson, Å., & Theorell, H. (1967) *Acta Chem. Scand. 21*, 1099–1101.